

Wear of Materials 2021

The Effect of Temperature on the Erosion of Polyurethane Coatings for Wind Turbine Leading Edge Protection --Manuscript Draft--

Manuscript Number:	WOM2021-D-20-00007
Article Type:	Research Paper
Section/Category:	Erosion and Erosion-Corrosion
Keywords:	Polymers; coatings; Solid particle erosion; Nanoindentation; Profilometry; Wind turbines
Corresponding Author:	Mike Godfrey University of Southampton UNITED KINGDOM
First Author:	Mike Godfrey
Order of Authors:	Mike Godfrey Oliver Siederer Jurgita Zekonyte Ismail Barbaros Robert Wood
Abstract:	<p>Wind turbine leading-edge erosion can degrade the aerodynamic properties of blades and reduce their efficiency. Previous theoretical work has suggested that low temperatures might affect the erosion performance of leading-edges and protective leading-edge coatings. This study investigated solid particle erosion which is caused by dust, sand and hailstones impacting the leading edges. For polymer coatings, temperature is a particular concern; the low temperatures can cause a transition from ductile to brittle failures. Polyurethane (PU) coatings were eroded at two temperatures: ambient (25°C) and cold (-30°C). An adapted solid-air erosion facility was used to accelerate sub-angular sand particles of 96.2 µm mean size to a velocity of 68±8 m/s. Low volumetric sand concentrations of 1.3×10⁻⁴ % were studied at two impingement angles of 45 and 90 degrees. The results showed that cold temperatures influenced the erosion rate and erosion mechanism of the coatings, with the erosion rate at the cold temperature increasing significantly. The erosion classification values and the shape of the wear scar suggested plastic erosion behaviour of the PU at cold temperatures, as opposed to the more erosion-resistant elastic behaviour. A temperature-controlled nanoindentation study demonstrated that the ratio of hardness to modulus reduced and the plasticity index increased with a reduction in temperature, implying the PU coatings had an increased propensity to plastically deform during cold erosion. This supports the erosion performance seen in experiments; however, the cold erosion surfaces developed more pits than the ambient case. Cross-section analysis of the eroded coatings showed accumulation of damage subsurface with evidence of delamination at the weakest interfaces in the layered coating systems, across all temperatures.</p>

Highlights

- Solid particle erosion of polyurethane coatings for leading edge protection.
- Erosive resistance was significantly impaired at low temperatures.
- Erosion mechanism was more ductile at low temperatures.
- Nanoindentation showed plasticity index increased with temperature decrease.
- Irrespective of temperature, subsurface cracking of polyester layer was prevalent.

THE EFFECT OF TEMPERATURE ON THE EROSION OF POLYURETHANE COATINGS FOR WIND TURBINE LEADING EDGE PROTECTION

Mike Godfrey^{a,*}, Oliver Siederer^a, Jurgita Zekonyte^a, Ismail Barbaros^a, Robert Wood^a

^a *nCATS, Faculty of Engineering and Physical Sciences, University of Southampton, SO17 1BJ, UK*

July 2020

Abstract

Wind turbine leading-edge erosion can degrade the aerodynamic properties of blades and reduce their efficiency. Previous theoretical work has suggested that low temperatures might affect the erosion performance of leading-edges and protective leading-edge coatings. Solid particle erosion is caused by dust, sand and hailstones impacting the leading edges. For polymer coatings, temperature is a particular concern; the low temperatures can cause a transition from ductile to brittle failures. Polyurethane (PU) coatings were eroded at two temperatures: ambient (25°C) and cold (-30°C). An adapted solid-air erosion facility was used to accelerate sub-angular sand particles of 96.2 µm mean size to a velocity of 68±8 m/s. Low volumetric sand concentrations of 1.3×10⁻⁴ % were studied at two impingement angles of 45 and 90 degrees. The results showed that cold temperatures influenced the erosion rate and erosion mechanism of the coatings, with the erosion rate at the cold temperature increasing significantly. The erosion classification values and the shape of the wear scar suggested plastic erosion behaviour of the PU at cold temperatures, as opposed to the more erosion-resistant elastic behaviour. A temperature-controlled nanoindentation study demonstrated that the ratio of hardness to modulus reduced and the plasticity index increased with a reduction in temperature, implying the PU coatings had an increased propensity to plastically deform during cold erosion. This supports the erosion performance seen in experiments; however, the cold erosion surfaces developed more pits than the ambient case. Cross-section analysis of the eroded coatings showed accumulation of damage subsurface with evidence of delamination at the weakest interfaces in the layered coating systems, across all temperatures.

Keywords: Polymers, Coatings, Solid particle erosion, Nanoindentation, Profilometry, Wind turbines

1 INTRODUCTION

Wind turbine leading-edge erosion caused by rain, hail and airborne particles can result in a loss of annual energy production of up to 25% and, in some cases, structural damage to the blade itself [1,2]. Therefore, leading edges need to be designed to withstand high-velocity impingement. (A typical 5 MW wind turbine has a rated wind speed of 11 m/s; a tip speed ratio of between 6 and 8 equates to a tip velocity of 66-88 m/s [3,4].) One solution to this problem is to coat the blades in a thermoplastic polyurethane (TPU).

TPUs have recently gained interest as a material suitable for erosion-resistant coatings [5–12]. TPUs are classified as ductile elastomers with numerous advantages over many alternative erosion-resistant coatings; they have good corrosion resistance, good adhesion to the substrate and are lighter than their metallic or ceramic counterparts [11].

* Corresponding author. Engineering, University of Southampton, Highfield, Southampton, SO17 1BJ, United Kingdom.

Email addresses: mrg1g16@soton.ac.uk (M. Godfrey), Jurgita.Zekonyte@port.ac.uk (J. Zekonyte), r.wood@soton.ac.uk (R. Wood),

Research relating to wind turbine blade wear has generally focused on rain erosion; however, solid particles can also cause damage [13]. For this reason, this paper presents a study based on solid particle erosion. Some key previous studies into the erosion of PU are outlined in **table 1**.

Table 1: Previous studies into the wear of polyurethane

Reference	Temperature studied	Details of study	Year
[5]	63–67°C	Experimental, liquid medium	2001
[6]	-20 °C, 23°C, 60°C, 100°C	Theoretical	2013
[8]	Not specified	Experimental	1990
[10]	Room temperature implied	Experimental	1990
[12]	-100–150°C	Theoretical	2014
[14]	25°C, 60°C, 100°C	Experimental	2016
[15]	22°C, 60°C, 100°C	Theoretical	2017

S.W. Zhang et al (2001) [5] studied the abrasive erosion of PU in liquid mediums, a low impingement velocity (9.1 m/s), a particle size of 300–450 μm and a relatively high temperature (63–67°C). They found the erosion mechanism was a combination of microcutting, plastic fracture and corrosion and the elevated temperature caused chemical changes, such as thermal degradation of the allophanate and biuret groups, hydrolysis and surface oxidative degradation.

As well as experimentally determining the effect of thickness of a TPU coating on erosive wear, N. Zhang et al (2013) [6] theoretically modelled the effect of temperature on the erosion resistance of TPUs at four temperatures between -20°C and 100°C. This research predicted that the erosion rate of TPUs is lower at 23°C than at -20°C. This difference in erosion resistance was attributed to the decrease in temperature, increasing Young's Modulus and decreasing yield strain and stress [5],[8]. This was further substantiated by previous work that had found erosion rate increases as the temperature difference between the testing temperature and the glass transition temperature reduces [16]. The erosion itself also causes a temperature increase, due to the conversion of kinetic energy into plastic work and thermal energy. N. Zhang et al (2013) [6] showed this with temperatures of up 70°C being recorded 1 mm below the TPU surface and a simulated prediction of 76°C at the surface with ambient surroundings.

I. M. Hutchings et al (1990) [8] showed that there is a good correlation between rebound resilience and erosion resistance. On the other hand, J. Li et al (1990) [10] found that other material properties influenced the erosion rate of PU, such as hardness, tensile modulus and tensile strength even for similar values of rebound resilience. It has also been suggested that viscoelastic properties play an important role in the erosion behaviour of PU and that the loss modulus of PU varies significantly with temperature [12,17]. H. Ashrafizadeh et al (2016, 2017) studied the temperature dependence on the erosive performance of PU both experimentally [14] and theoretically [15] but only at elevated temperatures.

Depending on the material, solid particle erosion may occur through a brittle mechanism (cracking) or a ductile mechanism (cutting or ploughing) - although some materials, such as polymers, often exhibit a more complex mechanism. Elastomers generally wear by tearing and fatigue, with cracking perpendicular to the erosion direction [7–9]. This complex combination of mechanisms makes predicting the life of these coatings difficult [18]. The layers and interfaces underneath the PU coating also play an important role in the wear performance. Stress waves transmitted into the substrate can result in delamination [19]. S. W. Zhang et al. (1995) [20] suggests that the cohesive energy between the surface layer and substrate is minimised where the local temperature is the highest, which results in fatigue delamination in polyurethanes. Local temperature increase from particle impact can also decrease the strength of the surface. For this reason, increasing the thermal conductivity of PU has been investigated [21].

The erosion rate is dependent on many factors. These may relate to either the erodent or the target material. The former includes the kinetic energy of the impinging particles, the number of particles, erodent shape, erodent size, impingement angle and the flow regime [22],[23],[24]. Target material properties, such as hardness, tensile modulus and tensile strength, have been shown to affect the erosive properties of a system [10].

Ductile and brittle erosion mechanisms have different angular dependences. As a result of this, the profile of an erosion scar is dependent on the erosion mechanism: a ductile mechanism generating a W-shaped scar and a brittle mechanism generating a U-shaped scar [25]. H. Wensink et al (2002) [26] introduced the erosion classification value (E_C value or E_{CV}) to indicate whether the angular dependence demonstrated ductile or brittle erosion characteristics. This value is calculated by dividing the erosion rate at 45° by the erosion rate at 90° (equation 1).

$$E_{cv} = \frac{\left(\frac{dM_{loss}}{dM_{erodent}} \right)_{45}}{\left(\frac{dM_{loss}}{dM_{erodent}} \right)_{90}} \quad (1)$$

Where M_{loss} is the target material mass loss and $M_{erodent}$ is the cumulative mass of impinged erodent.

For ductile materials, $E_{CV} > 1$, while, for brittle materials, $E_{CV} \approx 0.45$. Thus, for ductile materials the erosion rate at 45° is greater than or equal to the rate at 90° and brittle materials exhibit faster erosion with orthogonal impingement. An initial period of mass gain, from embedded erodent, can be observed for soft, ductile materials. This is referred to as the incubation period and occurs most prominently at high angles of attack, with normal impacts having the greatest incubation period if it exists for that material [27,28]. Plastics have been found to have a greater incubation period compared to other ductile materials like metals [27].

While there have been several studies of erosion at ambient and elevated temperatures, including those of TPU, few study the effect of low temperatures and none have done so experimentally. Motivation to implement wind turbines in cold environments arises from the increase in air density at low temperatures; air at -30°C is 26.7% denser than at 35°C and the power output of a wind turbine is proportional to air density [9]. In extreme cases, wind turbines installed in areas such as Whitehorse, Canada can see temperatures dip to less than -30°C [29].

The objective of this study was to assess the erosive wear performance of PU-based wind turbine blade coatings at a low temperature (-30°C) and determine how the erosion mechanism differs between cold and ambient erosion.

2 METHODOLOGY

2.1 EROSION EXPERIMENT

The erosion tests were carried out using the high-velocity air-sand jet impingement erosion facility at the University of Southampton [30]. Air was compressed, desiccated and guided through a nozzle onto the specimen surface. Sand was fed into the air stream from a vibrating ramp. The sand feed time was controlled by a built-in timer. Between each erosion interval, the specimen was removed from the erosion test machine, allowed to reach ambient temperature (for the cold tests), then cleaned with paper towels and compressed air. The specimen was then weighed to a resolution of 10 μg using a precision balance. Weighing of specimens after each erosion interval was repeated at least four times. To change the impingement angle, the specimen was tilted in the fixture. The internal diameter of the acceleration tube was 20 mm; similar to the diameter of the wear scar, suggesting negligible particle-particle interactions in the stream. An airflow rate of 200 m^3/hr was used which equates to a particle velocity of $68 \pm 8 \text{ m/s}$ according to the latest calibration.

The system was modified to cool the stream by brazing a cryogenic nozzle onto the side of the main nozzle, enabling the introduction of a cryogenic liquid (nitrogen) into the main gas stream. A visual inspection found it was fully vaporised by the time it reached the specimen. A thermocouple attached to the back of the specimen was connected to a PID controller which regulated the liquid nitrogen flow rate via an on/off solenoid valve. The apparatus is outlined in [figure 1](#).

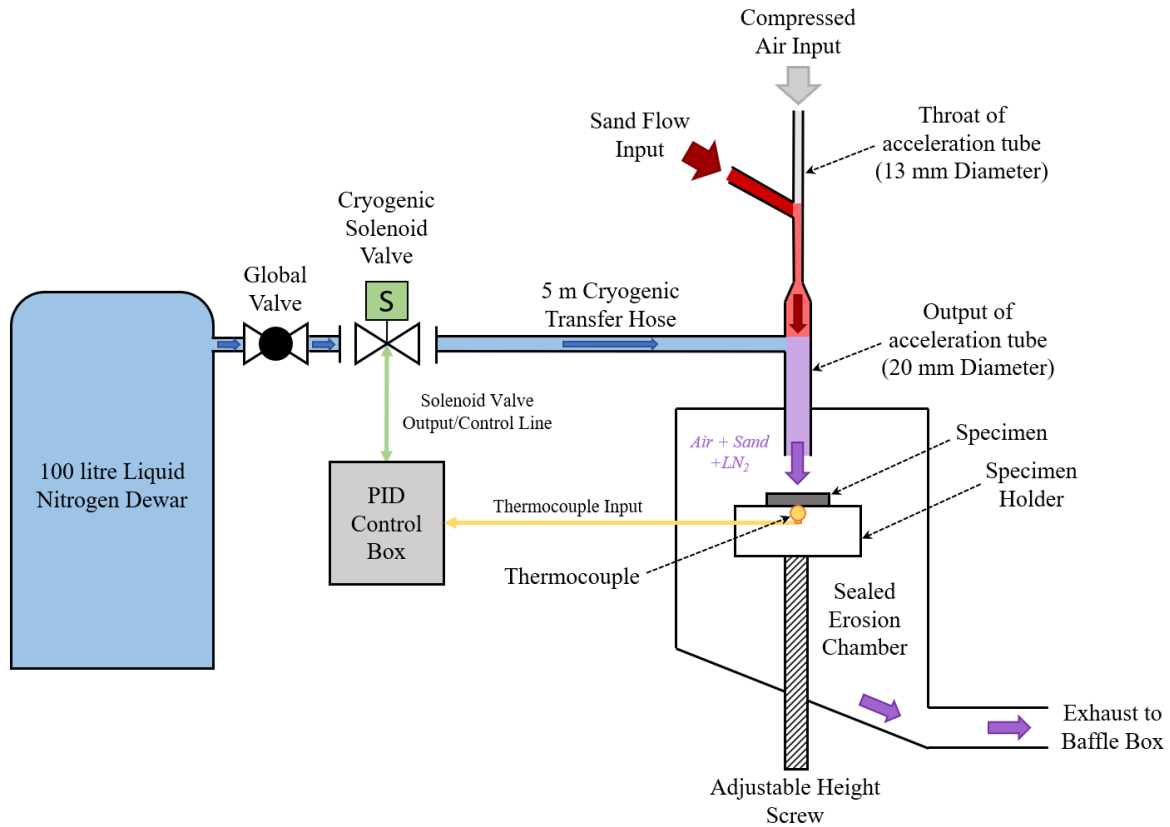


Figure 1: A diagram of the modified high-velocity air-sand jet impingement erosion facility.

A temperature calibration was performed without erodent. A specimen was mounted with two thermocouples: one fixed to the upper surface of the specimen and one fixed to the back. To achieve a surface temperature of $-30^\circ\text{C} (\pm 10^\circ\text{C})$, the back of the specimen was maintained at -17°C via the PID controller ([figure 2](#)).

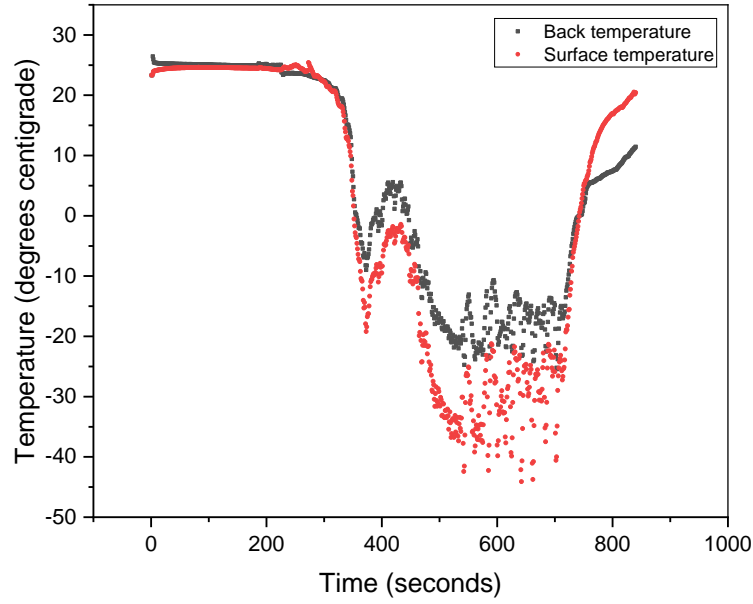


Figure 2: Temperature change of a specimen as liquid nitrogen was introduced into the air stream. Note that the peak at 430 seconds was due to a global valve adjustment.

Quartz (silicon dioxide) sand was used as the erodent (sourced from Hepworth Minerals, Redhill, Surrey, UK). An optical micrograph of the erodent is shown in figure 3. Based on the Wentworth scale, the erodent is categorised as very fine sand.

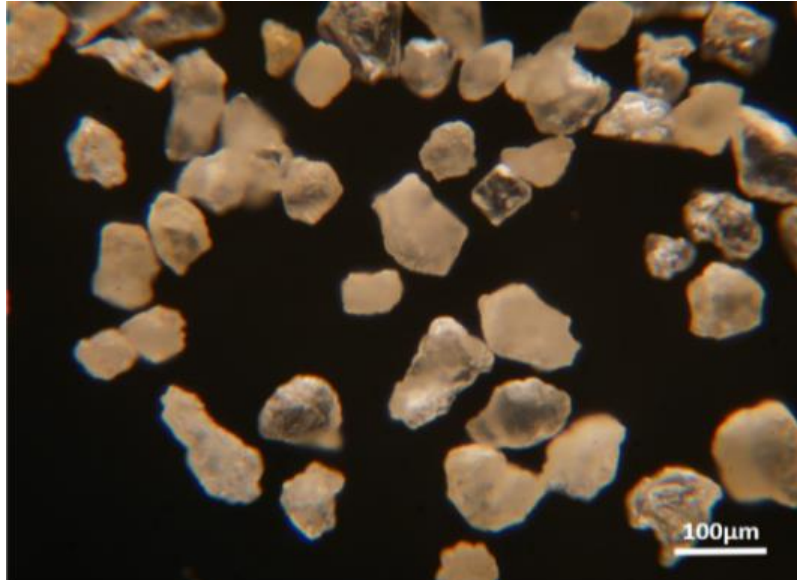


Figure 3: An optical micrograph of the erodent.

A random sample of 171 sand grains was measured using optical microscopy. The properties of the erodent are summarised in table 2. Properties are expressed in both microns and the Krumbein phi scale, calculated with equation 2.

$$\phi = -\log_2 \left(\frac{D}{D_0} \right) \quad (2)$$

Where ϕ is the phi value, D is the diameter of the sand particle in mm and D_0 is a reference diameter, equal to 1 mm.

Table 2: A summary of the erodent properties

Mean particle size	96.2 μm (ϕ size = 3.6)
Standard deviation of particle size	45.9 μm (ϕ units = 0.9)
Mean roundness	0.3 (Sub-angular)
Mean sphericity	0.7

The erodent size distribution is shown in figure 4.

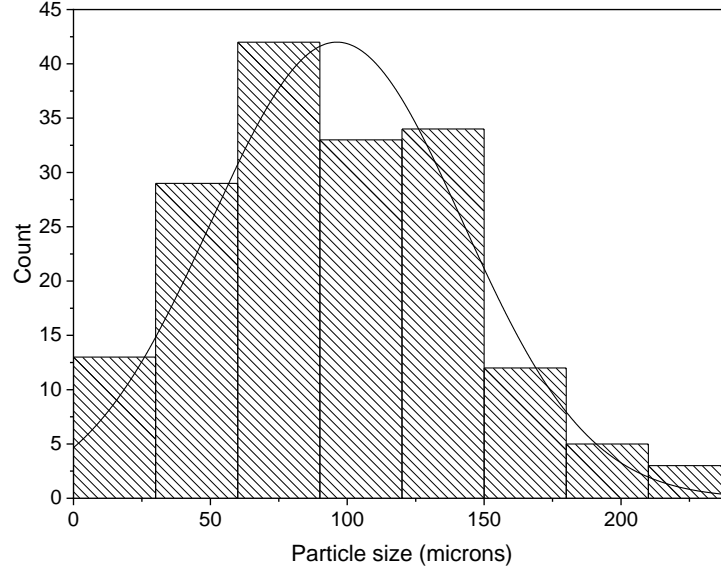


Figure 4: A histogram displaying the particle size distribution of the erodent.

2.2 NANOINDENTATION EXPERIMENT

Nanoindentation on various coatings was performed using a Nano Test Vantage instrument (Micro Materials Ltd., Wrexham, UK) at low temperatures (room temperature, +10, +5, +2.5, 0, -2.5, -5, -10°C). Indentations were performed using a Berkovich diamond indenter in load-controlled mode. The maximum loading force was set to 1 mN; loading/unloading time was set to 20 s. A dwell time of 30 s was set at maximum load to reduce the influence of creep. 10 indents with a spacing of 30 μm were done at each temperature.

The Vantage system uses Peltier cooling to separately cool both the sample stage and the indenter to the required temperature. A thermocouple was attached to measure the temperature at the top of the specimen surface. The indenter and specimen were brought into contact when the defined temperature on both the tip and surface was reached. A 300 s thermalization time was set before each indentation cycle. All temperature-dependent indentation experiments were carried out in a nitrogen-purged atmosphere to prevent the formation of ice crystals.

The data was analysed using the Oliver-Phar method [31] using analytical software provided by Micro Materials.

2.3 SAMPLES

The TPU coatings were applied to a fibreglass substrate. The first was a commercial brush-on PU blade coating (PB): three layers were applied. The PB coating also consisted of a polyester (PE) layer underneath the TPU layer. The second coating was a tape made by 3M (product number W8607) one layer of 3M tape was applied to the substrate. Both coatings were 0.4 mm thick. Each specimen was cut to 45 mm x 50 mm x 2 mm thick.

3 RESULTS AND DISCUSSION

The erosion rate can be observed from the gradient of the linear regions in the graphs shown in figure 5. (Error bars cannot be resolved against the scale of the graphs, so errors are omitted from figure 5 and presented in figure 6 instead).

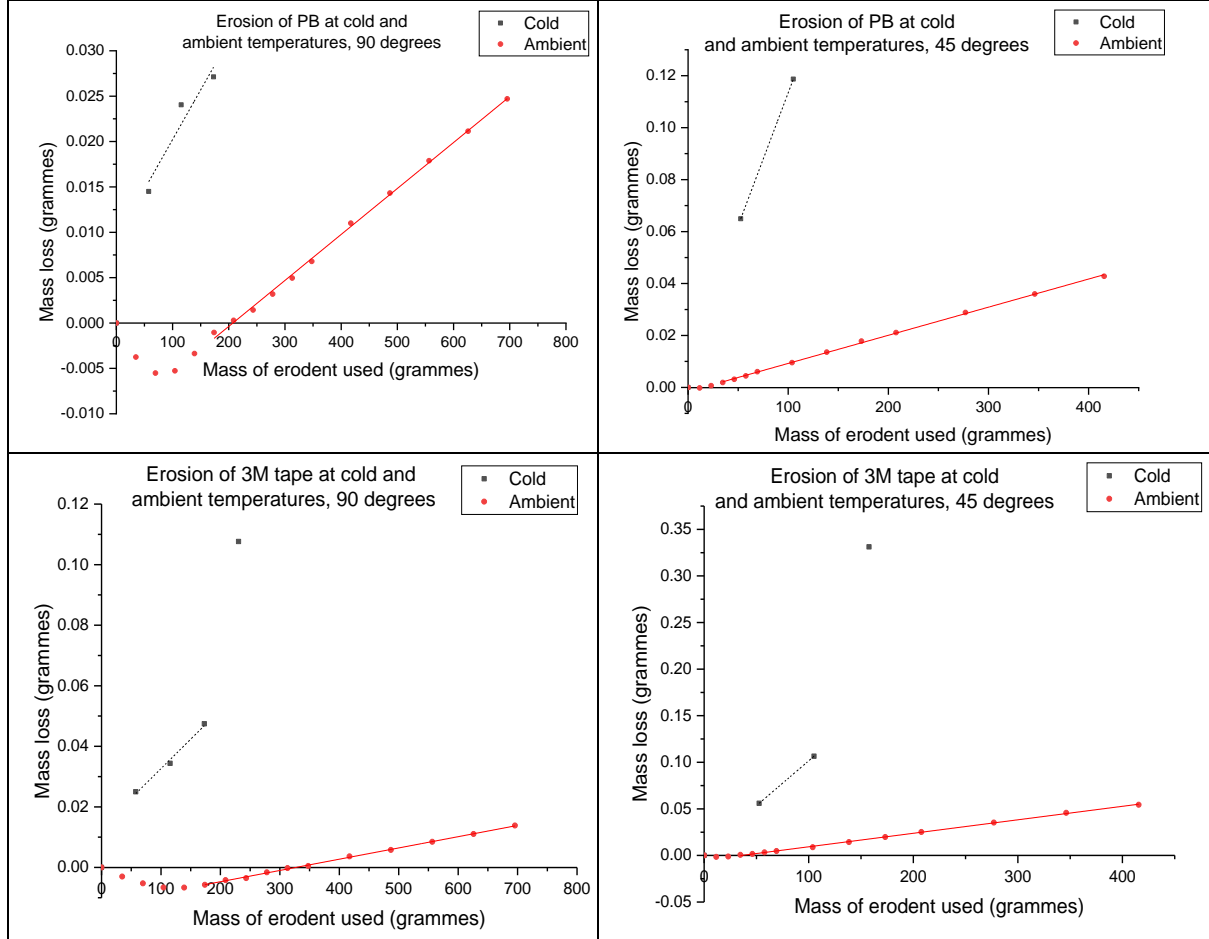


Figure 5: Mass loss vs mass of erodent used. PB with a 90° impingement angle (top left), PB with a 45° impingement angle (top right), 3M with a 90° impingement angle (bottom left), 3M with a 45° impingement angle (bottom right). Note the scales change.

Figure 6 shows the erosion rate increased significantly for the reduced temperature. In the case of the 45° impingement PB case, the erosion rate increased by over 9 times. The conversion from mass-loss to the volumetric loss per particle impact (E) was determined using equation 3, assuming each impinging particle was spherical.

$$E = \frac{\pi D_p^3 \rho_p \dot{M}_s}{6 \rho_s \dot{M}_p} \quad (3)$$

Where D_p is the mean diameter of the particle (96.2 μm), ρ_p is the particle density (2648 kgm^{-3}), \dot{M}_s is the steady-state mass loss rate from the specimen, ρ_s is the sample coating density (1250 kgm^{-3}) and \dot{M}_p is the erodent mass flow rate (10.51-11.59 g/min, depending on the test).

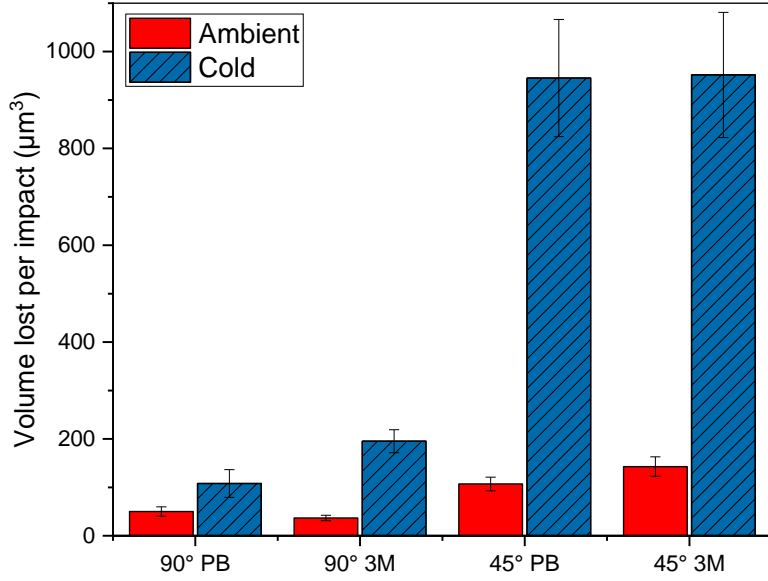


Figure 6: A bar chart comparing the steady-state erosion rates of the different samples at ambient and cold temperatures.

The uncertainties in the erosion rate shown as error bars in figure 6 were calculated using Monte-Carlo error approximation with 1×10^5 iterations. The following uncertainties were used: the standard error in particle diameter was $3.51 \mu\text{m}$, the uncertainty in particle density was 20 kgm^{-3} , the standard deviation in sample weight measurement was $38.5\text{-}300 \mu\text{g}$ (depending on the test), the uncertainty in TPU density was 25 kgm^{-3} and the standard deviation of erodent mass flow rate was $0.06\text{-}0.78 \text{ g/min}$ (depending on the test).

The orthogonal ambient erosion tests were repeated, and the erosion rates agreed to less than 3%. The 3M cold oblique impingement test was also repeated, albeit the repeat was shortened; the cold tests agreed with a discrepancy of less than 5%.

Using the erosion rates presented in figure 6, the E_C values for each scenario were calculated and are presented in table 3. The increase of E_C values for the cold scenario suggests that the erosion mechanism became more ductile at colder temperatures.

Table 3: E_C of samples, unitless

PB, ambient	PB, cold	3M tape, ambient	3M tape, cold
2.14 ± 0.19	8.76 ± 1.14	3.89 ± 0.28	4.88 ± 0.24

The kinetic energy of an individual particle and the energy dissipated in the coating was calculated with equations 4 and 5 respectively.

$$K_E = \frac{2}{3} \pi \left(\frac{D_p}{2} \right)^3 \rho_p v_p^2 = \frac{2}{3} \pi \left(\frac{96.2 \times 10^{-6}}{2} \right)^3 \times 2648 \times 68^2 = 2.85 \mu\text{J} \quad (4)$$

$$E_d = K_E (1 - \varphi^2) \quad (5)$$

Where D_p is the particle diameter ($96.2 \mu\text{m}$), ρ_p is the particle density (2648 kgm^{-3}), v_p is the particle velocity (68 m/s) and φ is the coefficient of restitution (COR) at that angle of impingement (0.4 for orthogonal impingement and 0.8 for oblique impingement).

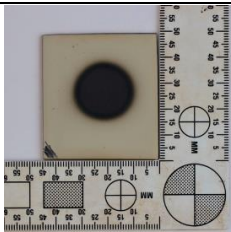
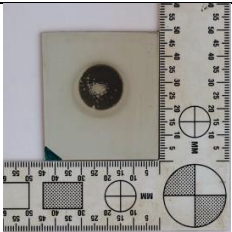
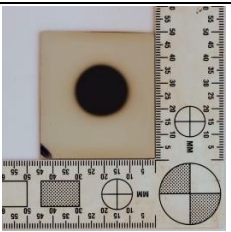
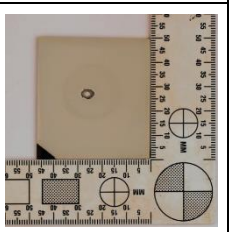
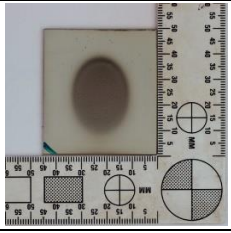
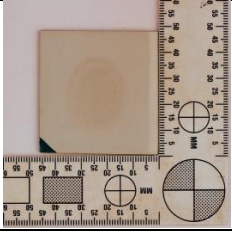
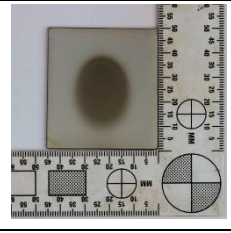
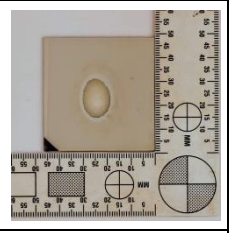
The energy calculations are summarised in table 4, including energy dissipated normalised by mass loss to allow a comparison between each scenario. The total energies were calculated from the product of the individual particle energy and the predicted number of impacts.

Table 4: A summary of energy calculations.

Impact angle	Experiment	Erosion time (minutes)	Total mass loss (g)	Total Impact energy (kJ)	Total energy dissipated (kJ)	Total energy dissipated/mass loss (kJ/g)
Orthogonal	Ambient PB	60	0.02471	1.61	1.35	54.58
	Ambient 3M	60	0.01384	1.61	1.35	97.45
	Cold PB	15	0.02712	0.40	0.34	12.37
	Cold 3M	15	0.04744	0.39	0.33	6.95
Oblique	Ambient PB	36	0.04277	0.96	0.35	8.07
	Ambient 3M	36	0.05439	0.96	0.35	6.35
	Cold PB	10	0.11870	0.26	0.09	0.79
	Cold 3M	15	0.10655	0.36	0.13	1.23

Table 5 contains photographs of each specimen post-test. Despite the shorter erosion durations used for the cold specimens, significantly more damage is visible after cold erosion, including the presence of numerous large pits, and wear through to the substrate, in the case of the 3M tape.

Table 5: Specimen images after erosion

	PB		3M tape	
	Ambient	Cold	Ambient	Cold
Orthogonal				
	1 hour	15 minutes	1 hour	20 minutes
Oblique				
	36 minutes	10 minutes	36 minutes	15 minutes

The optical micrographs shown in figure 7 demonstrate significantly different surfaces between ambient and cold erosion.

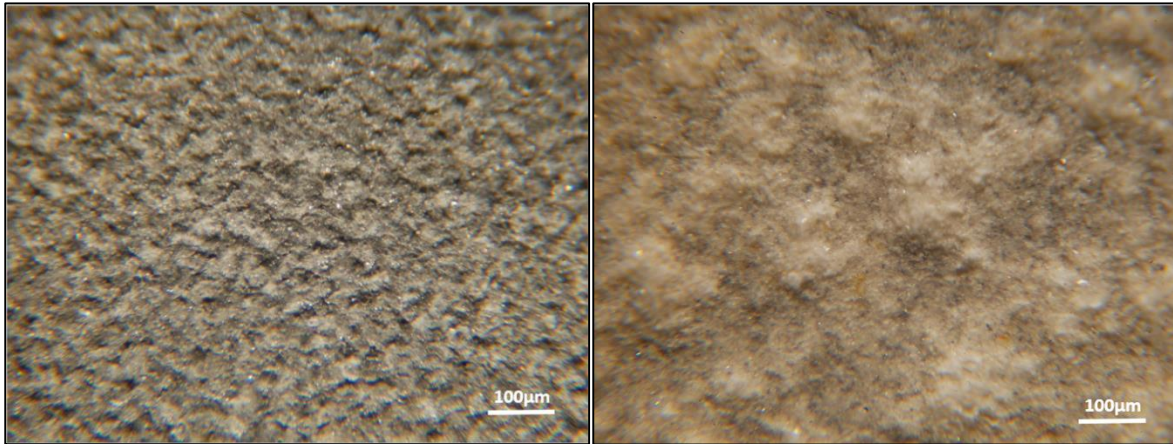


Figure 7: Optical micrographs of a PB specimen after 5 minutes of erosion at a 90° impingement angle. Ambient (left), cold (right).

Figure 8 shows a pit approximately 100 µm in diameter formed after cold erosion; pitting was not present after ambient erosion. Particles about 10 µm in size can be seen in figure 8 suggesting embedded particles were present in the cold case, but not measurable gravimetrically.

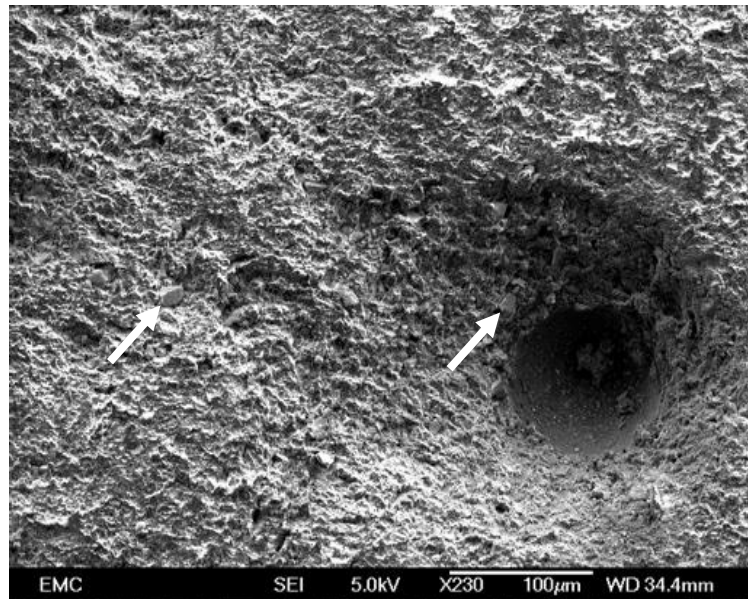


Figure 8: A scanning electron micrograph of a pit formed in the PB coating after 15 minutes of cold erosion. Arrows point to two examples of sand fragments.

Figure 9 shows optical micrographs of sections through the centre of the scar for the PB specimen taken for the orthogonal impingement case. Cracking of the PE layer is observed in both the cold and ambient cases. The thickness of the PU layer is also seen to be significantly reduced after cold erosion; this correlates with the mass data.

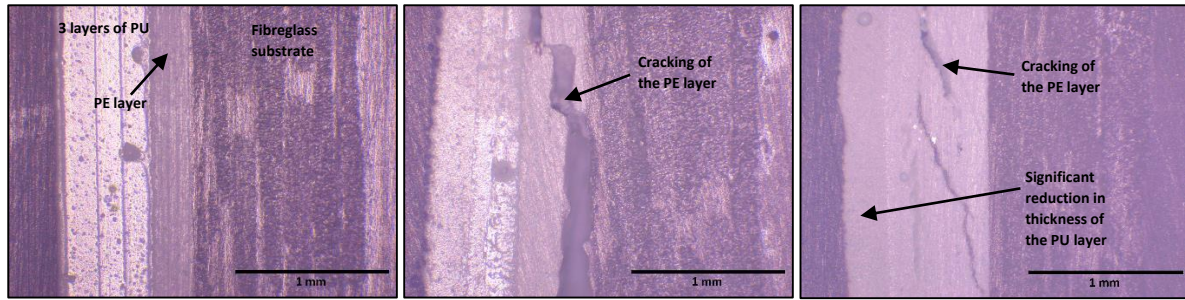


Figure 9: Optical micrographs of sections for the PB specimen. Left: uneroded. Middle: ambient eroded with orthogonal impingement for 1 hour. Right: cold eroded with orthogonal impingement for 15 minutes.

The scar profiles were measured using a Taylor-Hobson Talysurf and are shown in figures 10-13. They show that the profile is smooth for the ambient case, whereas the cold case has significant pits showing the increased risk of wear to the substrate (note the difference in depth scale). Even if the substrate is not damaged, the main purpose of the coating (preserving blade aerodynamics) is compromised. The scar profile shapes suggest more brittle erosion behaviour (U-shaped) at the higher temperature and more ductile (W-shaped) at the low temperature; this concurs with the E_c values shown in table 3.

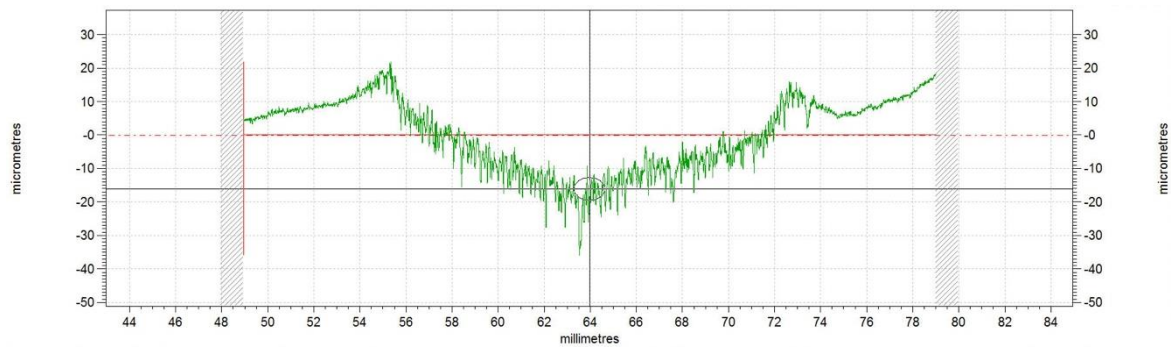


Figure 10: The scar profile of a PB specimen eroded at ambient temperature at 90° for 15 minutes.

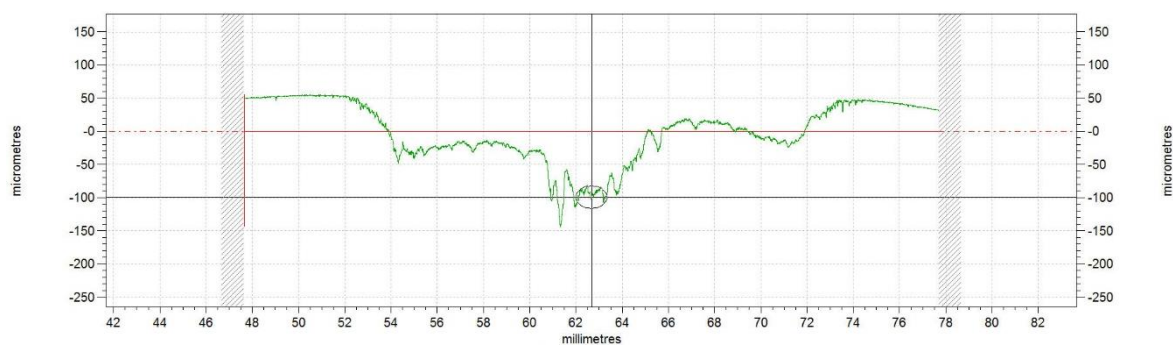


Figure 11: The scar profile of a PB specimen eroded at cold temperature at 90° for 15 minutes.

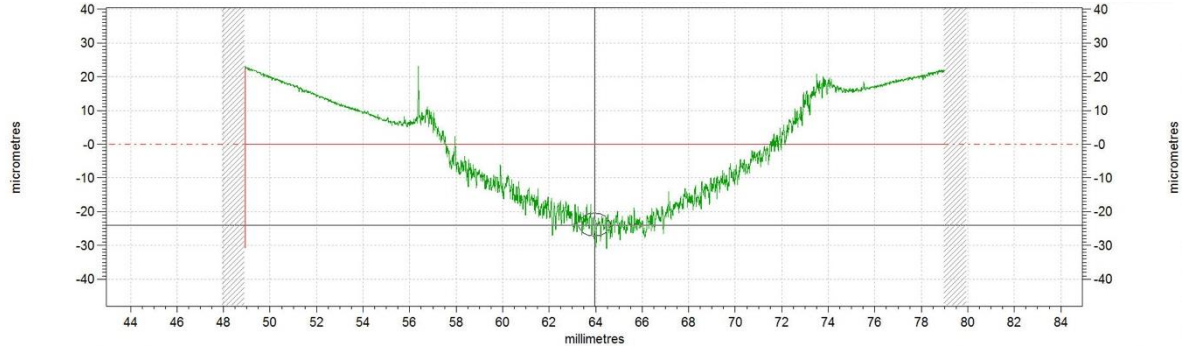


Figure 12: The scar profile of a 3M specimen eroded at ambient temperature at 90° for 20 minutes.

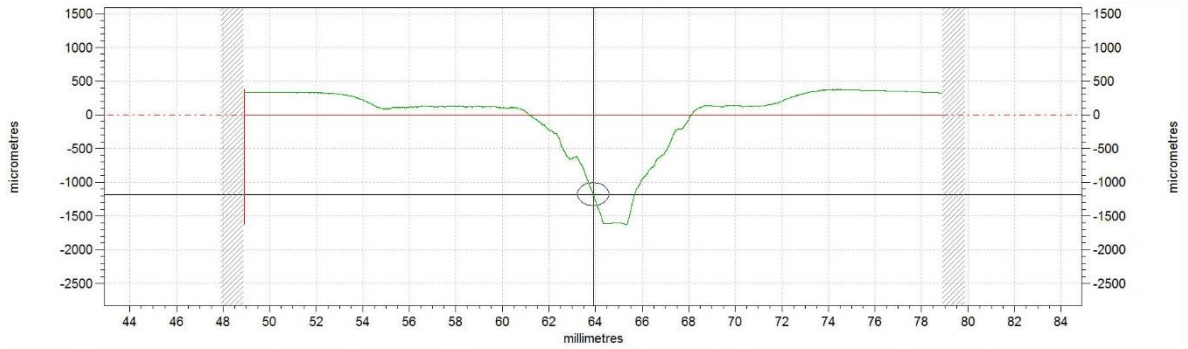


Figure 13: The scar profile of a 3M specimen eroded at cold temperature at 90° for 20 minutes. Erosion to the substrate can be observed.

The nanoindentation study showed an increase in hardness, H , and reduced modulus, E_r , with decreasing temperature on all coatings (figure 14). The glass transition temperature for the coatings is between -5 and +5°C. As expected, the biggest changes in values were observed within this range and even lower temperatures, where polymers are locked in their glassy state.

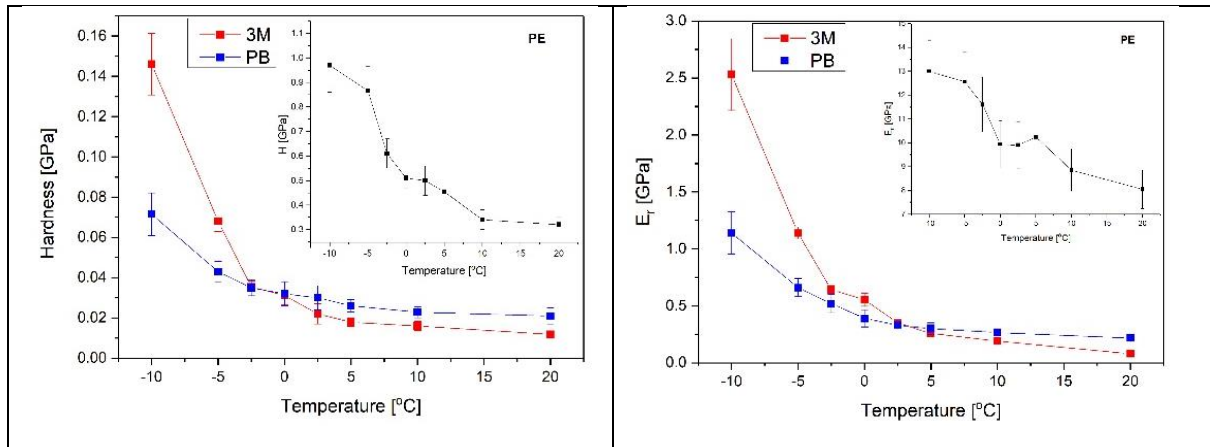


Figure 14: Hardness (left) and Reduced Modulus (right) as a function of temperature for three coatings.

The ratio of hardness to modulus (H/E_r) was demonstrated to be a useful value that characterises the mechanical behaviour of coatings [32–34]. H/E_r is also linked to the dimensionless “plasticity index” (PI) [34] that determines the limit of elastic behaviour. At higher H/E_r ratios (i.e. lower PI), resistance to plastic deformation is increased and thus, so is the expected wear resistance. Figure 15 shows a significant reduction in the H/E_r ratio and an increase in the plasticity index in the PU-based coatings as the temperature reduced, implying an increased propensity to demonstrate plastic behaviour at lower temperatures. This material behaviour agrees with the erosion results observed in the E_c values

presented in table 3. The plastic behaviour explains the increase in erosion rate at lower temperatures as PU anti-erosion coatings rely on their elasticity.

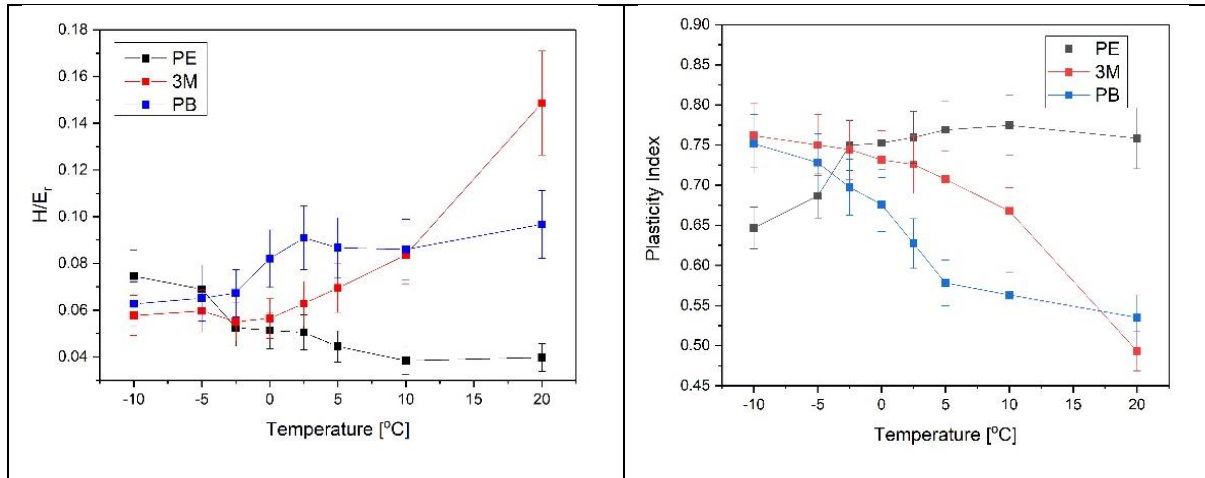


Figure 15: H/E_r ratio (left) and Plasticity Index (right) as a function of temperature for three coatings.

This study demonstrates the increased risk of wind turbine coating failure in cold climates. It is consequently vital that blade inspections be conducted more frequently on turbines installed in cold environments. This research has also shown that the erosion mechanism is more ductile at low temperatures, as demonstrated by the E_c values, wear scars and nanoindentation. The design of the next-generation erosion-resistant coatings can, therefore, use temperature-controlled nanoindentation tests to help predict the erosive wear at a range of temperatures, with the aim to reduce the dependence of H/E_r and PI upon temperature, compared to current TPU coatings. Irrespective of temperature, this research has also shown cracking of the PE layer beneath the PU coating leading to potential delamination issues. Future coating designs should address this issue.

4 CONCLUSION

4.1 KEY RESULTS

- The erosion rate was far greater during the cold (-30°C) erosion tests than ambient (25°C) erosion tests.
- The E_c values and erosion scars suggested the erosion mechanism was more ductile at the cold temperature.
- More pitting was observed during the cold tests.
- Sectioning revealed substantial cracking of the PE layer underneath the PU in both the ambient and cold cases.
- Significant abrasion of the PU layer occurred during cold erosion but not during ambient erosion.
- Nano-indentation studies revealed that the PI increased with a reduction in temperature and the H/E_r ratio reduced with temperature. To improve anti-erosion performance, a coating with properties that have less temperature-dependence should be selected.

4.2 LIMITATIONS AND FURTHER WORK

- The cold tests were run at an extreme operating temperature. A range of temperatures should be tested to enable a better understanding of the effect of temperature of the erosion performance of the coatings.
- The nanoindentation study measured down to -10°C. A further study with a larger temperature range would allow a better understanding of how the material properties change with temperature.

5 ACKNOWLEDGEMENTS

This work was supported by Windtrust with an EU FP7 funded collaboration [grant number number 322449]. The authors would like to acknowledge Dr Jellio Bello, whose technical expertise with the erosion facility was crucial for the completion of the project. They also thank Thom Bostock, Robert Loades and Dr Wendell Bailey for their help organising the cryogenic aspect of the project. A big thank you goes to Dr Charlie Burson-Thomas, Dr Terry J Harvey, Dr Simon Dennington, Hazel Mitchell and Charlie Godfrey for their general help and advice.

6 REFERENCES

- [1] A. Sareen, C.A. Sapre, M.S. Selig, Effects of leading edge erosion on wind turbine blade performance, *Wind Energy*. 17 (2014) 1531–1542. <https://doi.org/10.1002/we.1649>.
- [2] S. Zhang, K. Dam-Johansen, S. Nørkjær, P.L. Bernad, S. Kiil, Erosion of wind turbine blade coatings - Design and analysis of jet-based laboratory equipment for performance evaluation, *Prog. Org. Coatings*. 78 (2015) 103–115. <https://doi.org/10.1016/j.porgcoat.2014.09.016>.
- [3] Z. Jiang, M. Karimirad, T. Moan, Dynamic response analysis of wind turbines under blade pitch system fault, grid loss, and shutdown events, *Wind Energy*. 17 (2013). <https://doi.org/10.1002/we.1639>.
- [4] N. Çetin, M. Yurdusev, R. Ata, A. Özdamar, Assessment of Optimum Tip Speed Ratio of Wind Turbines, *Math. Comput. Appl.* 10 (2005) 147–154. <https://doi.org/10.3390/mca10010147>.
- [5] S.W. Zhang, R. He, D. Wang, Q. Fan, Abrasive erosion of polyurethane, *J. Mater. Sci.* 36 (2001) 5037–5043. <https://doi.org/10.1023/A:1011814506377>.
- [6] N. Zhang, F. Yang, L. Li, C. Shen, J. Castro, L.J. Lee, Thickness effect on particle erosion resistance of thermoplastic polyurethane coating on steel substrate, *Wear*. 303 (2013) 49–55. <https://doi.org/10.1016/j.wear.2013.02.022>.
- [7] P.J. Slikkerveer, M.H.A. van Dongen, F.J. Touwslager, Erosion of elastomeric protective coatings, *Wear*. 236 (1999) 189–198. [https://doi.org/10.1016/S0043-1648\(99\)00268-9](https://doi.org/10.1016/S0043-1648(99)00268-9).
- [8] J.C. Arnold, I.M. Hutchings, The mechanisms of erosion of unfilled elastomers by solid particle impact, *Wear*. 138 (1990) 33–46. [https://doi.org/10.1016/0043-1648\(90\)90166-8](https://doi.org/10.1016/0043-1648(90)90166-8).
- [9] N. Dalili, A. Edrisy, R. Carriveau, A review of surface engineering issues critical to wind turbine performance, *Renew. Sustain. Energy Rev.* 13 (2009) 428–438. <https://doi.org/10.1016/j.rser.2007.11.009>.
- [10] J. Li, I.M. Hutchings, Resistance of cast polyurethane elastomers to solid particle erosion, *Wear*. 135 (1990) 293–303. [https://doi.org/10.1016/0043-1648\(90\)90032-6](https://doi.org/10.1016/0043-1648(90)90032-6).
- [11] P.G. Cizmas, J.C. Slattery, Dimensionless correlation for sand erosion of families of polymers, *Wear*. 262 (2007) 316–319. <https://doi.org/10.1016/j.wear.2006.05.008>.
- [12] D. Acierno, L. Sanguigno, G. Arena, K. Friedrich, E. Padenko, P. Russo, Erosion behavior and mechanical properties of thermoplastic polyurethanes, in: *AIP Conf. Proc.*, American Institute of Physics Inc., 2014: pp. 110–113. <https://doi.org/10.1063/1.4876790>.
- [13] L. Bartolomé, J. Teuwen, Prospective challenges in the experimentation of the rain erosion on the leading edge of wind turbine blades, *Wind Energy*. 22 (2019) 140–151. <https://doi.org/10.1002/we.2272>.
- [14] H. Ashrafizadeh, P. Mertiny, A. McDonald, Evaluation of the effect of temperature on

- mechanical properties and wear resistance of polyurethane elastomers, (2016).
<https://doi.org/10.1016/j.wear.2016.08.008>.
- [15] H. Ashrafizadeh, A. McDonald, P. Mertiny, Development of a finite element model to study the effect of temperature on erosion resistance of polyurethane elastomers, *Wear*. 390–391 (2017) 322–333. <https://doi.org/10.1016/j.wear.2017.08.009>.
 - [16] A.I. Marei, P. V Izvozhnikov, Determination of the wear of rubbers in a stream of abrasive particles, in: *Abrasion of Rubber*, MacLaren London, 1967: pp. 274–280.
 - [17] G. Arena, K. Friedrich, D. Acierno, E. Padenko, P. Russo, G. Filippone, J. Wagner, Solid particle erosion and viscoelastic properties of thermoplastic polyurethanes, *Express Polym. Lett.* 9 (2015) 166–176. <https://doi.org/10.3144/expresspolymlett.2015.18>.
 - [18] H.M. Slot, E.R.M. Gelinck, C. Rentrop, E. Van Der Heide, Leading edge erosion of coated wind turbine blades: Review of coating life models, *Renew. Energy*. 80 (2015) 837–848. <https://doi.org/10.1016/j.renene.2015.02.036>.
 - [19] E. Cortés, F. Sánchez, L. Domenech, A. Olivares, T.M. Young, A. O’Carroll, F. Chinesta, Manufacturing issues which affect coating erosion performance in wind turbine blades, in: *AIP Conf. Proc.*, American Institute of Physics Inc., 2017. <https://doi.org/10.1063/1.5008010>.
 - [20] S.W. Zhang, W. Deguo, Y. Weihua, Investigation of abrasive erosion of polymers, *J. Mater. Sci.* 30 (1995) 4561–4566. <https://doi.org/10.1007/BF01153063>.
 - [21] H. Ashrafizadeh, A. McDonald, P. Mertiny, Erosive and Abrasive Wear Resistance of Polyurethane Liners, in: *Asp. Polyurethanes*, InTech, 2017. <https://doi.org/10.5772/intechopen.68870>.
 - [22] R.J.K. Wood, The sand erosion performance of coatings, *Mater. Des.* 20 (1999) 179–191. [https://doi.org/10.1016/s0261-3069\(99\)00024-2](https://doi.org/10.1016/s0261-3069(99)00024-2).
 - [23] M. Naveed, H. Schlag, F. König, S. Weiß, Influence of the Erodent Shape on the Erosion Behavior of Ductile and Brittle Materials, *Tribol. Lett.* 65 (2017) 1–9. <https://doi.org/10.1007/s11249-016-0800-x>.
 - [24] S. Bahadur, R. Badruddin, Erodent particle characterization and the effect of particle size and shape on erosion, *Wear*. 138 (1990) 189–208. [https://doi.org/10.1016/0043-1648\(90\)90176-B](https://doi.org/10.1016/0043-1648(90)90176-B).
 - [25] D.W. Wheeler, R.J.K. Wood, Erosion of hard surface coatings for use in offshore gate valves, in: *Wear*, Elsevier, 2005: pp. 526–536. <https://doi.org/10.1016/j.wear.2004.03.035>.
 - [26] H. Wensink, M.C. Elwenspoek, A closer look at the ductile–brittle transition in solid particle erosion, *Wear*. 253 (2002) 1035–1043. [https://doi.org/10.1016/S0043-1648\(02\)00223-5](https://doi.org/10.1016/S0043-1648(02)00223-5).
 - [27] G.P. Tilly, Erosion caused by airborne particles, *Wear*. 14 (1969) 63–79. [https://doi.org/10.1016/0043-1648\(69\)90035-0](https://doi.org/10.1016/0043-1648(69)90035-0).
 - [28] I.M. Hutchings, *Tribology: Friction and Wear of Engineering Materials*, Edward Arnold, Great Britain, 1992.
 - [29] J.F. Maissan, P. Eng, *Wind Power Development in Sub-Arctic Conditions with Severe Rime Icing*, Whitehorse, 2001.
 - [30] R.J.K. Wood, D.W. Wheeler, Design and performance of a high velocity air–sand jet impingement erosion facility, *Wear*. 220 (1998) 95–112. [https://doi.org/10.1016/S0043-1648\(98\)00196-3](https://doi.org/10.1016/S0043-1648(98)00196-3).
 - [31] W.C. Oliver, G.M. Pharr, An improved technique for determining hardness and elastic modulus using load and displacement sensing indentation experiments, *J. Mater. Res.* 7 (1992) 1564–1583. <https://doi.org/10.1557/JMR.1992.1564>.

- [32] J. Musil, F. Kunc, H. Zeman, H. Poláková, Relationships between hardness, Young's modulus and elastic recovery in hard nanocomposite coatings, *Surf. Coatings Technol.* 154 (2002) 304–313. [https://doi.org/10.1016/S0257-8972\(01\)01714-5](https://doi.org/10.1016/S0257-8972(01)01714-5).
- [33] A. Leyland, A. Matthews, On the significance of the H/E ratio in wear control: A nanocomposite coating approach to optimised tribological behaviour, *Wear.* 246 (2000) 1–11. [https://doi.org/10.1016/S0043-1648\(00\)00488-9](https://doi.org/10.1016/S0043-1648(00)00488-9).
- [34] B.D. Beake, G.S. Fox-Rabinovich, S.C. Veldhuis, S.R. Goodes, Coating optimisation for high speed machining with advanced nanomechanical test methods, *Surf. Coatings Technol.* 203 (2009) 1919–1925. <https://doi.org/10.1016/j.surfcoat.2009.01.025>.